Charge-dependent directed flows in heavy-ion collisions by Boltzmann-Maxwell equations

Jun-Jie Zhang,[1] Xin-Li Sheng,[2] Shi Pu,[3] Jian-Nan Chen,[1] Guo-Liang Peng,[4,1] Jian-Guo Wang,[1,5] and Qun Wang[3]

[1]*Northwest Institute of Nuclear Technology, Xi'an 710024, China*

[2]*Key Laboratory of Quark and Lepton Physics (MOE) and Institute of Particle Physics, Central China Normal University, Wuhan 430079, China*

[3]*Department of Modern Physics, University of Science and Technology of China, Hefei 230026, China*

[4]*Beijing Institute of Technology, Beijing 100081, China*

[5]*School of Information and Communications Engineering, Xi'an Jiaotong University, Xi'an 710049, China*

(Received 4 February 2022; revised 28 June 2022; accepted 29 July 2022; published 22 August 2022)

We have calculated the directed flow v_1 and charge-dependent directed flow Δv_1 of pions and protons in Au+Au collisions at $\sqrt{s_{NN}} = 200$ GeV by solving the coupled Boltzmann-Maxwell equations self-consistently. Our numerical results show that v_1 for pions and protons are all negative in the positive midrapidity region and have similar behavior and magnitude. In contrast we find a quite different behavior in Δv_1 for pions and protons. The difference lies in that Δv_1 for protons mainly comes from pressure gradients of the medium, while the dominant contribution to Δv_1 for pions is from electromagnetic fields. Our results indicate that the effect of the electric field will slightly exceed that of the magnetic field and lead to a small negative slope of Δv_1 for pions.

DOI: 10.1103/PhysRevResearch.4.033138

I. INTRODUCTION

The quantum matter under strong electromagnetic (EM) fields is an old, but still thriving, research area in many disciplines of physics. Strongly coupled quark-gluon plasma (QGP), a new state of matter governed by quantum chromodynamics, has been produced and extensively studied in high-energy heavy-ion collisions for decades at the Relativistic Heavy Ion Collider (RHIC) of Brookhaven National Lab and at the Large Hadron Collider (LHC) of the European Organization for Nuclear Research (CERN). In the early stage of heavy-ion collisions, extremely strong EM fields of the order of 10^{18}–10^{19} gauss are generated [1–3], which leaves an imprint on the subsequent evolution of the QGP (for recent reviews of heavy-ion collisions and QGP, see, e.g., Refs. [4–6]). Strong EM fields lead to many novel quantum phenomena such as the chiral magnetic effect [7,8] and the chiral magnetic wave [9,10] in heavy-ion collisions (for recent reviews of these effects, see Refs. [11,12]).

Studying these effects requires a self-consistent description of EM fields coupled to the medium. For example, precise information about the evolution of EM fields is crucial to extract the Chiral Magnetic Effect (CME) signals [12–15] and has been searched for a decade. EM fields from spectators were well described in previous studies [3,16–22] but not for the parts from the medium produced in collisions because it is difficult to describe the medium effects from first principles with unknown transport properties of the strongly coupled medium and complicated interaction between EM fields and medium particles. The fully self-consistent treatment of EM fields and the interacting medium may help unveil the physics and even puzzles behind these phenomena. As far as we know, due to great numerical challenges, the exact space-time evolution of EM fields has not been achieved.

One such example is the puzzle related to the directed flow v_1 and the charge-dependent directed flow Δv_1 [23]. The directed flow [24,25] is defined as $v_1 \equiv \langle \cos(\phi - \Phi_{\rm RP}) \rangle$ and reflects the collective sideward deflection of particles [26,27], with ϕ and $\Phi_{\rm RP}$ denoting the azimuthal angle of an outgoing particle and that of the reaction plane, respectively. The charge-dependent directed flow is defined as $\Delta v_1^h \equiv v_1(h^+) - v_1(h^-)$, which is the difference between the directed flows of charged particles and their antiparticles, and is expected to be sensitive to the EM field due to the opposite EM forces exerted on particles with opposite charges. Currently, both the hydrodynamical and transport models give a similar pattern of v_1 which agrees with the experiments. However, the results for Δv_1 from hydrodynamical models [28–33] disagree with the measurement of Δv_1—the theoretical results show that both the pion's Δv_1^π and the proton's Δv_1^p in Au+Au collisions at $\sqrt{s_{NN}} = 200$ GeV have negative slopes, while the STAR data for Δv_1^π show an almost vanishing slope and those for Δv_1^p have a positive slope [34]. The transport models [35–39] also give consistent results for Δv_1 for hadrons [34] at high energies, but it is challenging to include the EM effects self-consistently in these models. Therefore, the influence of the electromagnetic fields on the evolution of the system is important [40].

To reconcile the disagreement, it is essential to perform a fully self-consistent calculation of the QGP evolution coupled to the Maxwell equations. Most previous studies either treat

EM fields as background fields without back-reactions from medium particles [28–30] or adopt a perturbation method with simplified distributions of EM fields and QGP [41].

In this work, we carry out a fully self-consistent simulation of the dynamical evolution of the QGP in EM fields by solving the relativistic Boltzmann equations coupled to the Maxwell equations on graphics processing units (GPUs) [42]. Our algorithm naturally incorporates all the electromagnetic effects, including the Lorentz, Coulomb, and Faraday effects. As a first test of our algorithm, we study the directed flow v_1 and its charge-dependent component Δv_1^h for pions and protons, trying to unveil the physics behind the Δv_1 puzzles. With the help of the state-of-the-art computing power of GPUs, we are also able to calculate the evolution of the EM fields in heavy-ion collisions in a more realistic and precise way, providing a more reliable baseline for many effects related to EM fields such as the CME effect.

II. METHODS

The dynamical evolution of the QGP in EM fields is described by the relativistic Boltzmann equation,

$$\left[p^\mu \partial_\mu + Q_a p_\mu F^{\mu\nu} \partial_\nu^p\right] f_a(t, \mathbf{x}, \mathbf{p}) = \mathcal{C}[f_a], \tag{1}$$

where f_a is the spin- and color-averaged distribution function of the parton a with $a = q, \bar{q}, g$ for the quark, antiquark, and gluon, respectively, and Q_a denotes its electric charge. The strong interaction among partons is encoded in the collision term $\mathcal{C}[f_a]$.[1] In the calculation we consider all 2-to-2 scatterings among u, d, and s quarks; their antiquarks; and gluons [45], and the thermal masses of partons in the matrix elements are chosen to be $m_{u,d,\bar{u},\bar{d}} = 0.3$ GeV, $m_{s,\bar{s}} = 0.5$ GeV, and $m_g = 0.5$ GeV. The EM field tensor $F^{\mu\nu}$ is determined by solving the Maxwell equations,

$$\begin{aligned} \partial_\mu F_{\alpha\beta} + \partial_\alpha F_{\beta\mu} + \partial_\beta F_{\mu\alpha} &= 0, \\ \partial_\mu F^{\mu\nu} &= j^\nu_{\text{ext}} + j^\nu_{\text{med}}, \end{aligned} \tag{2}$$

where the source of the EM field has two parts: the external current j^ν_{ext} and the medium current j^ν_{med}. The external current j^ν_{ext} is generated by fast-moving partons, including spectators and quarks in the rapidity range $|y| > 1$. The dynamical evolution of j^ν_{ext} is assumed to be decoupled from the EM field because the trajectories of these fast-moving particles are hardly influenced by the field. The medium current j^ν_{med} is from quarks in the midrapidity region,

$$j^\nu_{\text{med}} = \sum_{a=q,\bar{q}} Q_a N_a \int \frac{d^3\mathbf{p}}{(2\pi)^3} \frac{p^\nu}{E_a} f_a(t, \mathbf{x}, \mathbf{p}), \tag{3}$$

where $E_a \equiv \sqrt{\mathbf{p}^2 + m_a^2}$ is the energy of the parton with the mass m_a given above, N_a is the degeneracy factor counting the degrees of freedom of the spin and color ($N_q = N_{\bar{q}} = 6$ for quarks and $N_g = 16$ for gluons), and the sum runs over all quarks and antiquarks due to their nonzero electric charges. We see that j^ν_{med} leads to a coupling between the Boltzmann equation (1) and the Maxwell equations (2): the motion of quarks and antiquarks is influenced by the Coulomb and Lorentz forces from the EM field, while the EM field is generated by the motion of charged quarks and antiquarks.

We consider Au+Au collisions at $\sqrt{s_{NN}} = 200$ GeV. We assume that one gold nucleus moves along the $+z$ direction with its center located at $x = b/2$ and the other nucleus moves along the $-z$ direction with its center located at $x = -b/2$. We choose the Woods-Saxon distribution [47,48] as the initial *spatial* distribution for partons in the nucleus. The impact parameter is set to $b = 8$ fm, corresponding to 20%–30% centrality approximately. The initial *momentum* distribution at position $\mathbf{x}$ is inspired by the anisotropic distribution [49,50] of the color glass condensate [51–53],

$$f_a(t_0, \mathbf{x}, \mathbf{p}) = f_a^{(0)}\, r_q\, \theta\left(1 - \frac{\sqrt{\xi^2 p_z'^2 + \mathbf{p}_\perp'^2}}{Q_s}\right), \tag{4}$$

where $\mathbf{p}$ and $\mathbf{p}'$ are the three-momenta in the laboratory and local comoving frame, respectively, Q_s is the saturation scale [53,54], $t_0 \simeq 1/Q_s$ is the corresponding saturation time [55–57], and ξ is the anisotropy parameter [58]. Their values are chosen to be $Q_s = 1$ GeV, $t_0 \approx 0.2$ fm/c, and $\xi = 1.4$. In the overlap region of collisions only a fraction r_q of the participants are left in the midrapidity range $[-1, 1]$. We fix $r_q \simeq 0.1$ by making a comparison of the net charge distribution obtained in our simulation with that in the A Multi-Phase Transport model (AMPT) simulation. The coefficients $f_a^{(0)}$ for each species of quarks are determined by the corresponding quark number in the overlap region, i.e., $f_u^{(0)} = 0.996$, $f_d^{(0)} = 1.14$, and $f_s = 0$. Since there are no antiquarks initially, $f_{\bar{u},\bar{d},\bar{s}}^{(0)} = 0$. For gluons, we choose $f_g^{(0)} \simeq \alpha_s^{-1}/r_q$, which is inversely proportional to the coupling constant [59]. Note that, in the kinetic approaches, the initial quarks and gluons are treated as quasiparticles. The effect of the sea quarks is included as the thermal masses of the quarks and gluons. Only after about 0.2 fm/c, which is the reciprocal of the energy scale about 1 GeV, do the soft gluons interact and convert to quark antiquark pairs. The setup used in our paper is a typical initial condition in heavy-ion collisions (e.g., also see Refs. [41,55–57]).

We emphasize that only 10% of the initial partons in the overlap region, quantified by $r_q \simeq 0.1$, contribute to f_a and j^ν_{med} in the midrapidity region $[-1, 1]$. The remaining 90% of partons are assumed to follow the rapidity distribution $f^\pm(y) = e^{\pm y/2}/[4\sinh(y_{\text{beam}}/2)]$, with $1 < |y| < y_{\text{beam}}$, where $\pm$ correspond to the beam and target directions, respectively. Here $y_{\text{beam}} = 5.36$ is the beam rapidity for collisions at 200 GeV. The motion of these partons and spectators generates the external current j^ν_{ext} and thus provides a background EM field for the dynamical evolution of f_a.

In the hadronization stage, partons combine into hadrons in each phase space grid, whose yields agree with experimental data [60–62] for the rapidity density dN/dy for $\pi^\pm$, $K^\pm$, p, and $\bar{p}$ at the midrapidity $y = 0$.

[1] The collision term includes high-dimensional integrals which need a more efficient algorithm to calculate. These high-dimensional integrals are calculated by using the powerful numerical integration package ZMCintegral based on GPUs developed by some of us [43,44]. For more details, we refer readers to a previous work [45] by some of us. The EM field is also calculated on GPUs using Jefimenko's equations [46].

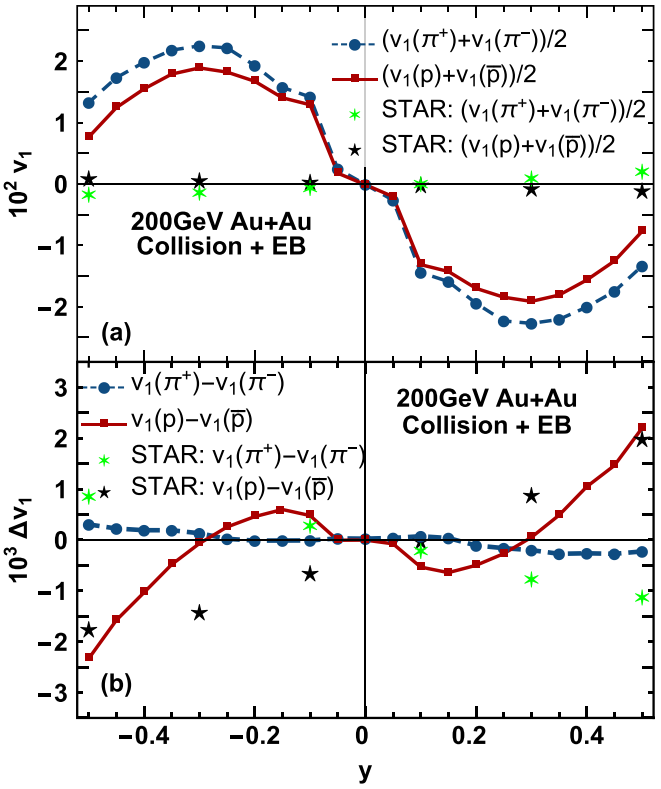

FIG. 1. (a) The directed flow v_1 and (b) charge-dependent directed flow Δv_1 as functions of the rapidity for protons/antiprotons (red solid line) and $\pi^{\pm}$ (blue dashed line) in Au+Au collisions at 200 GeV. The green and black stars are derived from STAR measurements for the 10%–40% centrality at 200 GeV Au+Au collisions [34]. Although our simulations correspond to the collisions in 20%–30% centrality, it is still observed that Δv_1 agrees with the data qualitatively. The values of the parameters are set to the saturation time $t = 0.2$ fm/c, the impact parameter $b = 8$ fm, the factor $r_q = 0.1$ in Eq. (4), the strong coupling constant $\alpha_s = 0.3$, and the range for transverse momenta $p_T \in [0.2, 1.5]$ GeV, and the distribution functions at $t = 5$ fm/c are used.

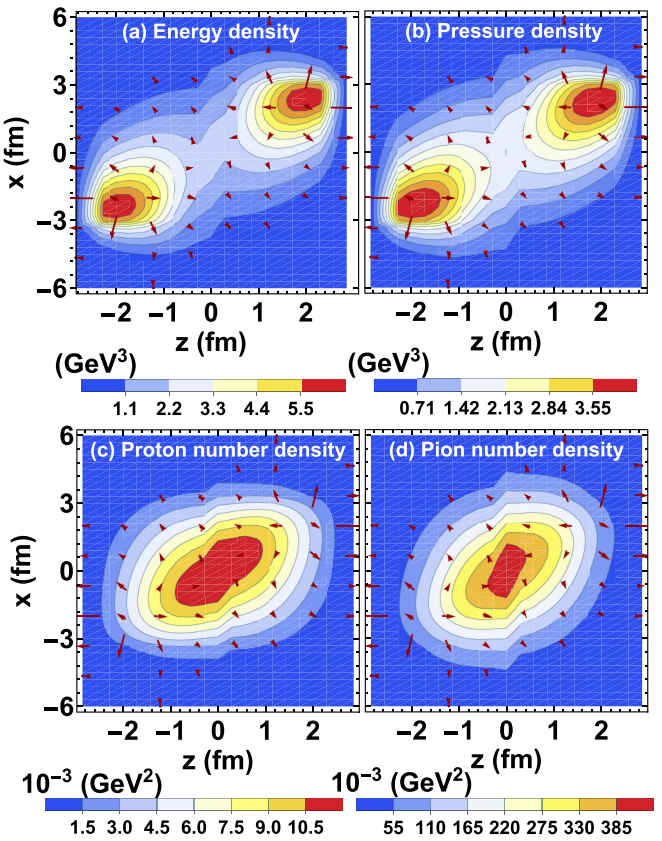

FIG. 2. Contour plots for (a) the energy density and (b) the pressure of all particles in the full rapidity and p_T range in the x-z plane. Contour plots for the number density of (c) protons (without antiprotons) and (d) pions in the ranges $y \in [-1, 1]$ and $p_T \in [0.2, 1.5]$ GeV in the x-z plane. The arrows stand for the directions of the pressure gradients formed by all particles (the same for all plots), and the distribution functions at t =2.5 fm/c are used. Other parameters are the same as in Fig. 1.

III. RESULTS

A. Negative slope of v_1

The calculated results for the directed flows as a function of rapidity for pions and protons in the range $p_T \in [0.2, 1.5]$ GeV are shown in Fig. 1(a). We see that v_1 for pions and protons have almost the same magnitude and are positive or negative in the $0.4 > y > 0$ or $0 > y > -0.4$ region, respectively. The evolution of the QGP governed by the strong interaction forms a tilted fireball in the reaction plane, as shown by the energy density and pressure of all particles in the full range of y and p_T in Figs. 2(a) and 2(b). The pressure gradients lead to an antiflow corresponding to a negative dv_1/dy at midrapidity [63–65].

To understand the generation of the antiflow, we plot in Figs. 2(c) and 2(d) the contours of the number density for protons and pions in the ranges $y \in [-1, 1]$ and $p_T \in [0.2, 1.5]$ GeV, which are mainly located in the central region. Due to pressure gradients, the protons at forward rapidity, which are mainly located in the $x \simeq 0$, $z > 0$ region, receive a force pointing in the bottom right direction and leading to a negative v_1. Similarly, protons at backward rapidity have a positive v_1.

We also notice the difference between our results and the STAR data in Fig. 1(a). First, our result for v_1 is more than 10 times larger than the experimental data, indicating a larger pressure gradient than in the experiments. We have studied the parameter dependence for v_1, such as the initial parton numbers $f_u^{(0)}$, $f_d^{(0)}$, and $f_g^{(0)}$; the coupling constant α_s; the size of the spatial grids; and the evolution time of the snapshot. We find that if more particles are involved in the initial condition (hence larger values for $f_u^{(0)}$, $f_d^{(0)}$, or $f_g^{(0)}$), a larger pressure gradient can be induced, leading to a larger magnitude of v_1. If we increase the coupling constant α_s, the system will evolve more like a fluid with stronger collective motions, which narrow the difference between p_x and p_y, thus leading to a smaller magnitude of v_1. The value of v_1 is not sensitive to the size of the spatial grids and the evolution time after 5 fm/c. Second, we observe that $|v_1(p) + v_1(\bar{p})| < |v_1(\pi^+) + v_1(\pi^-)|$ in our result, while the opposite behavior is found in the data. Such a difference may come mainly from the hadronization model since in the current study, we consider a simple coalescence hadronization model. To get a better understanding of v_1, a

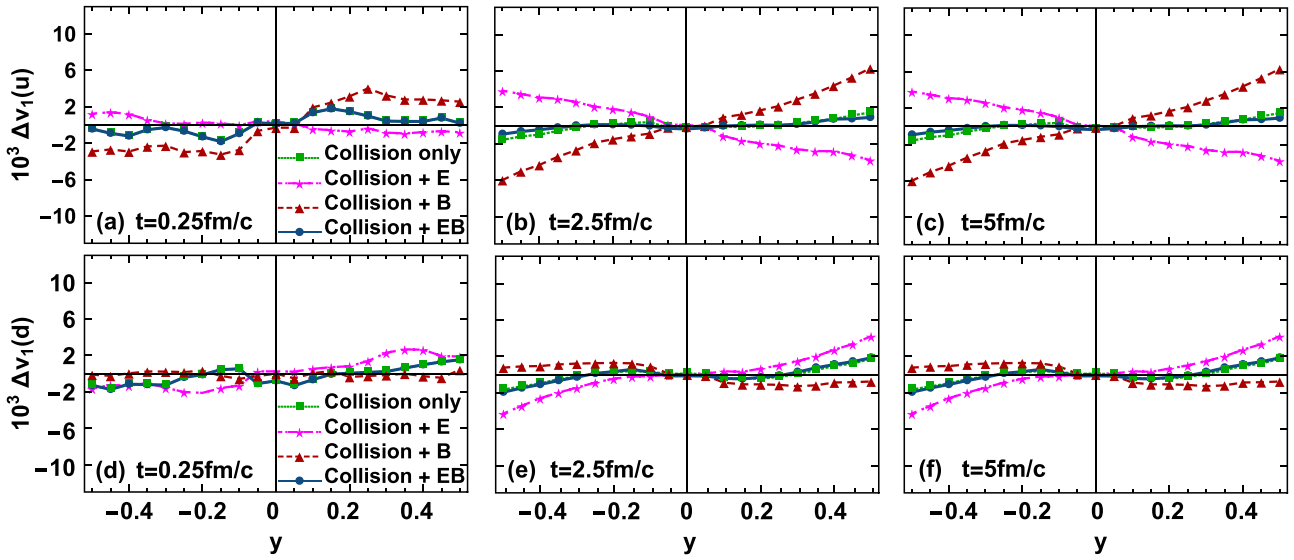

FIG. 3. Charge-dependent directed flow Δv_1 for (a)–(c) u and (d)–(f) d quarks at time $t = 0.25$, 2.5, 5.0 fm/c (left column, middle column, and right column). The green dotted, magenta dot-dashed, red dashed, and blue solid curves correspond to cases of only collision, collision with electric fields, collision with magnetic fields, and collision with both electric and magnetic fields, respectively. Other parameters are the same as in Fig. 1.

systematic study of the hadronization model in the current framework is required and will be presented elsewhere. Further discussion on the hadronization model at the quark level can be found in Sec. III D.

B. Different behaviors of Δv_1 for pions and protons

The results for charge-dependent directed flows Δv_1 for pions and protons are presented in Fig. 1(b). Since the dynamics of all charged quarks are governed by the same EM fields, a natural expectation is that Δv_1 for pions and protons as a function of rapidity should be similar, which has been observed in studies of hydrodynamics incorporating the EM fields [28–30]. However, we find in our study that Δv_1^p has a positive slope, while Δv_1^π has a very small negative slope. The reason why we observe a little negative slope of Δv_1^p in the rapidity range $[-0.2, 0.2]$ might due to the oversimplified model of the hadronization process. In Fig. 3, we do not observe such a phenomenon at the quark level.

How do we understand such counterintuitive results for Δv_1 for pions and protons? In fact, the different behaviors of Δv_1^π and Δv_1^p come from an interplay of pressure gradients and EM fields.

The positive slope for Δv_1^p is mainly attributed to pressure gradients, similar to the difference between $v_1(\pi^+) + v_1(\pi^-)$ and $v_1(p) + v_1(\bar{p})$, as shown in Fig. 1. Antiprotons as newly produced particles are more likely to appear in the region with higher energy densities and therefore larger pressure gradients as observed in Fig. 2. Therefore, the negativity for $v_1(\bar{p})$ is enhanced relative to $v_1(p)$. Such an effect exists even when the EM fields are switched off. In Fig. 4, we turn off the EM fields and plot Δv_1 caused by only collisions. We observe that Δv_1^π almost vanish but Δv_1^p still have positive slopes. On the other hand, the EM fields will influence the evolution of the QGP and therefore modify the pressure distribution as well as the number density distribution of hadrons, which finally results in an amplification of the Δv_1^p slope. Our results for Δv_1^p qualitatively agree with the Ultra-relativistic Quantum Molecular Dynamics model (UrQMD) simulation [66,67] and the data for the STAR experiment at RHIC [34]. But our results are quantitatively smaller than the data because the pressure induced by $j^\nu_{\rm ext}$ in Eq. (2) is neglected in this work.

The approximately vanishing Δv_1^π in Fig. 4(a) indicates that the splitting between π^+ and π^- in the transverse plane is a cumulative result of the EM fields. The small negative slope of Δv_1^π in Fig. 1(b) is consistent with the results from hydrodynamics incorporating the EM fields [28–30]. Unlike the case of protons and antiprotons, π^+ and π^- receive similar contributions from pressure gradients since they have almost identical spatial distributions.

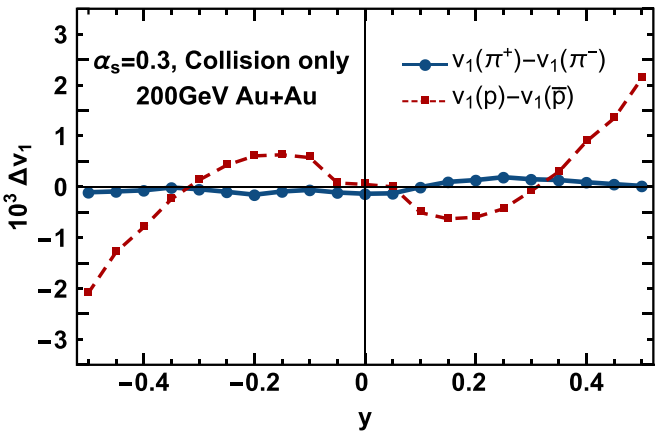

FIG. 4. Charge-dependent directed flow Δv_1^π and Δv_1^p as a function of rapidity with only collisions (without EM fields). The parameters are the same as in Fig. 1.

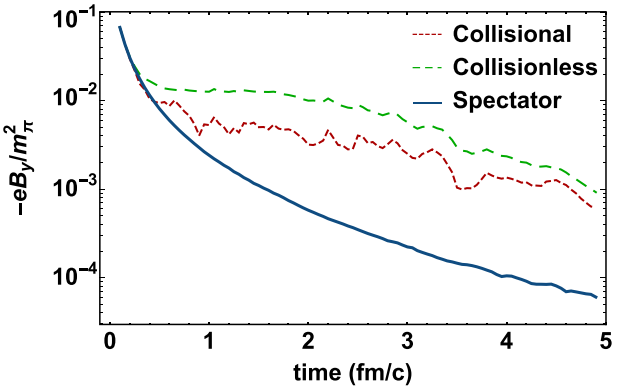

FIG. 5. The time evolution of magnetic fields in the central region of the reaction plane, $(x, y, z) = (0, 0, 0)$ fm. Other parameters are the same as in Fig. 1.

C. Δv_1 dependence on the p_T range

In Fig. 1(b), the transverse momentum is chosen in the range $p_T \in [0.2, 1.5]$ GeV. If, as discussed above, the behaviors of pions and protons in Δv_1 are from different mechanisms, the result should not be sensitive to the momentum range. To support this statement, we also calculate the dependence of Δv_1 on transverse momentum ranges. A parameter scan of the p_T range in the range $[x, 1.5]$ GeV, where $x \in \{0.2, 0.4, 0.6, 0.8, 1.0, 1.2\}$, shows that Δv_1 is not sensitive to the choice of transverse momentum range. We also observe that particles with p_T less than 1 GeV contribute little to the Δv_1 difference between pions and protons.

D. Δv_1 for quarks

A widely discussed issue for Δv_1^π is whether the contribution from the electric field is more important than that from the magnetic field [28–30]. To answer this question, we take a closer look at Δv_1 for quarks. We show the results of Δv_1^u and Δv_1^d as a function of rapidity in collisions with and without the electric (**E**) and magnetic (**B**) fields in Fig. 3 at three different times $t = 0.25,\ 2.5,\ 5.0$ fm/c.

For the case of only collision, different spatial distributions of u (d) and $\bar{u}$ ($\bar{d}$) give positive slopes for both Δv_1^u and Δv_1^d, which leads to the positive slope of Δv_1^p via hadronization.

The contributions from electric and magnetic fields to Δv_1 are opposite but of the same magnitude, which agrees with the theoretical result of Ref. [28]. Positively charged particles in forward rapidity are mainly influenced by the EM field from spectators with $B_y < 0$ and $E_x < 0$. Therefore, the magnetic force points in the $+x$ direction, while the electric force points in the opposite direction, so two forces partially cancel and lead to the net effect that is reflected in the difference of Δv_1 between the cases with and without the EM field, as shown in Fig. 3. We emphasize that the directed flow is a result of accumulation over time, so the balance of electric and magnetic contributions gradually changes with time. At an earlier time, e.g., $t = 0.25$ fm/c, Δv_1 is almost vanishing, which is the result of the cancelation of the electric and magnetic contributions, while the contribution from the electric field becomes larger at later time, e.g., $t = 5$ fm/c, and eventually, Δv_1 slightly favors the electric contribution. In Fig. 5, we present the evolution of the magnetic field in the central region of the reaction plane, in which the effects form collisions and medium partons can be clearly seen. Similar results can be found in Refs. [41,68].

Despite the hadronization model used in our simulation, we can understand the results via a simple sum rule in a naive picture of coalescence hadronization, i.e., a hadron's v_1 is approximately equal to the sum over v_1 of its constituent quarks [69–71]. To this end, we separate the contributions from EM fields and pressure gradients as $\Delta v_1^u \simeq 2\Delta v_1^{\rm EM} + \Delta v_1^{\rm pressure}$ and $\Delta v_1^d \simeq -\Delta v_1^{\rm EM} + \Delta v_1^{\rm pressure}$. The EM field contribution $\Delta v_1^{\rm EM}$ is proportional to the quark's charge, while the pressure contribution $\Delta v_1^{\rm pressure}$ is the same for all quarks, as shown in Fig. 3. Then following the coalescence sum rule, we have $\Delta v_1^\pi \simeq \Delta v_1^u - \Delta v_1^d \simeq 3\,\Delta v_1^{\rm EM}$ and $\Delta v_1^p \simeq 2\Delta v_1^u + \Delta v_1^d \simeq 3\,\Delta v_1^{\rm EM} + 3\Delta v_1^{\rm pressure}$, with their slopes in agreement with the results in Fig. 1. Meanwhile, we also find that the slopes of Δv_1 are insensitive to the coupling constant α_s.

E. Time variation of effective conductivity

An important quantity in the evolution of quark gluon plasma is the Ohmic conductivity. Since the system has not reached local thermal equilibrium, the conductivity is a

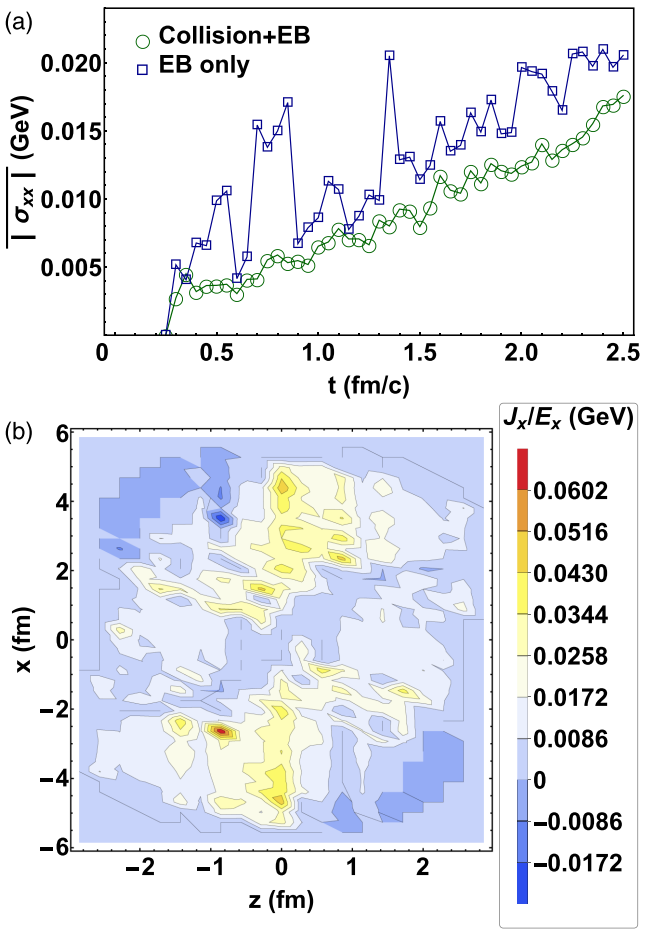

FIG. 6. (a) $\overline{|\sigma_{xx}|}$ at different time steps for two cases: one with collision and one without. (b) Spatial distribution of J_x/E_x in the reaction plane. Other parameters are the same as in Fig. 1.

tensor rather than a scalar. To perceive the presence of the conductivity, we define an effective conductivity $\sigma_{xx} = J_x/E_x$ which is a function of spatial positions. In Fig. 6(a), we show the time evolution of the average absolute value $\overline{|\sigma_{xx}|} = [\sum_{i,j} |\sigma_{xx}(x_i, y_j)|]/n$, where n denotes the number of grids in the reaction plane, which roughly reflects the amplitude of the Ohmic conductivity. We can see that when particle collisions are turned on, the conductivity is more stable with lower magnitude than the collisionless case, consistent with our expectation. In Fig. 6(b) we give the spatial distribution of σ_{xx} in the reaction plane at time 2.5 fm/c, from which we can see that σ_{xx} can be either positive or negative locally.

IV. DISCUSSION AND CONCLUSION

With the help of the state-of-the-art parallel computation algorithm, we are able to calculate the direct flow v_1 and charge-dependent direct flow Δv_1 for pions and protons in heavy-ion collisions by solving the coupled Boltzmann-Maxwell equations for QGP self-consistently. The collision configuration is set to Au+Au collisions at 200 GeV and 20%–30% centrality.

Our numerical results show that v_1 for pions and protons are all negative or positive in the $0.4 > y > 0$ or $0 > y > -0.4$ region, respectively, and have similar behaviors and magnitudes. The magnitude and behavior of v_1 for both protons and pions are different for the experimental data, suggesting that fine tuning of the parameters and a better hadronization model are required.

Our results for the slopes of Δv_1 at midrapidity are in qualitative agreement with the STAR data. We found that the positive slope of Δv_1 for protons comes mainly from pressure gradients in the fireball, while the small negative slope of Δv_1 for pions reflects the contribution from EM fields over a period of time. The electric and magnetic fields make opposite contributions to v_1 and Δv_1 but with the same magnitude. At a relatively later time, the electric effects will slightly exceed the magnetic effects, which gives rise to the small negative slope of Δv_1 for pions. Our results are insensitive to the values of the coupling constant and can be understood by a simple sum rule in a naive coalescence picture of hadronization.

To see clear effects from the EM fields, Δv_1 for D_0 and $\bar{D}_0$ mesons may be a better candidate, which requires increasing the number of momentum grids for heavy quarks. However, restricted by GPU resources, our current algorithm does not allow such a simple extension.

Our calculation can also give a prediction for $v_1(\pi^{\pm})$ in low-energy collisions. At the highest RHIC energy, no significant difference between $v_1(\pi^+)$ and $v_1(\pi^-)$ has been observed due to low statistical significance [34]. In lower-energy collisions, the EM fields will have a longer lifetime and therefore are expected to induce more sideward deflection for charged particles, i.e., a more negative slope of Δv_1^{π}. This qualitatively agrees with the experimental observation at 7.7, 11.5, and 19.6 GeV [34].

ACKNOWLEDGMENTS

We would like to thank H.-J. Xu for providing us with the charge rapidity distribution from AMPT to fix the parameters and U. Gürosy, K. Rajagopal and W.-B. Zhao for helpful discussions. The work is partly supported by the National Natural Science Foundation of China (NSFC) under Grants No. 12047528, No. 12075235, No. 12105227, and 12135011.

[1] V. Skokov, A. Y. Illarionov, and V. Toneev, Estimate of the magnetic field strength in heavy-ion collisions, Int. J. Mod. Phys. A **24**, 5925 (2009).

[2] A. Bzdak and V. Skokov, Event-by-event fluctuations of magnetic and electric fields in heavy ion collisions, Phys. Lett. B **710**, 171 (2012).

[3] V. Voronyuk, V. D. Toneev, W. Cassing, E. L. Bratkovskaya, V. P. Konchakovski, and S. A. Voloshin, Electromagnetic field evolution in relativistic heavy-ion collisions, Phys. Rev. C **83**, 054911 (2011).

[4] M. Gyulassy and L. McLerran, New forms of QCD matter discovered at RHIC, Nucl. Phys. A **750**, 30 (2005).

[5] D. H. Rischke, The quark gluon plasma in equilibrium, Prog. Part. Nucl. Phys. **52**, 197 (2004).

[6] W. Busza, K. Rajagopal, and W. van der Schee, Heavy ion collisions: The big picture, and the big questions, Annu. Rev. Nucl. Part. Sci. **68**, 339 (2018).

[7] D. E. Kharzeev, L. D. McLerran, and H. J. Warringa, The effects of topological charge change in heavy ion collisions: 'Event by event P and CP violation,' Nucl. Phys. A **803**, 227 (2008).

[8] K. Fukushima, D. E. Kharzeev, and H. J. Warringa, The chiral magnetic effect, Phys. Rev. D **78**, 074033 (2008).

[9] Y. Burnier, D. E. Kharzeev, J. Liao, and H.-U. Yee, Chiral Magnetic Wave at Finite Baryon Density and the Electric Quadrupole Moment of Quark-Gluon Plasma in Heavy Ion Collisions, Phys. Rev. Lett. **107**, 052303 (2011).

[10] D. E. Kharzeev and H.-U. Yee, Chiral magnetic wave, Phys. Rev. D **83**, 085007 (2011).

[11] D. E. Kharzeev, K. Landsteiner, A. Schmitt, and H.-U. Yee, Strongly interacting matter in magnetic fields: An overview, in *Strongly Interacting Matter in Magnetic Fields*, Lecture Notes in Physics Vol. 871 (Springer, Berlin, 2013), p. 1.

[12] D. E. Kharzeev, J. Liao, S. A. Voloshin, and G. Wang, Chiral magnetic and vortical effects in high energy nuclear collisions: A status report, Prog. Part. Nucl. Phys. **88**, 1 (2016).

[13] J. Zhao and F. Wang, Experimental searches for the chiral magnetic effect in heavy-ion collisions, Prog. Part. Nucl. Phys. **107**, 200 (2019).

[14] W. Li and G. Wang, Chiral magnetic effects in nuclear collisions, Annu. Rev. Nucl. Part. Sci. **70**, 293 (2020).

[15] M. S. Abdallah *et al.* (STAR Collaboration), Search for the chiral magnetic effect with isobar collisions at $\sqrt{s_{NN}} = 200$ GeV by the STAR collaboration at the BNL Relativistic Heavy Ion Collider, Phys. Rev. C **105**, 014901 (2022).

[16] V. D. Toneev, V. Voronyuk, E. L. Bratkovskaya, W. Cassing, V. P. Konchakovski, and S. A. Voloshin, Theoretical analysis of a possible observation of the chiral magnetic effect in Au + Au

collisions within the RHIC beam energy scan program, Phys. Rev. C **85**, 034910 (2012).
[17] W.-T. Deng and X.-G. Huang, Event-by-event generation of electromagnetic fields in heavy-ion collisions, Phys. Rev. C **85**, 044907 (2012).
[18] K. Tuchin, Time and space dependence of the electromagnetic field in relativistic heavy-ion collisions, Phys. Rev. C **88**, 024911 (2013).
[19] S. Pu, V. Roy, L. Rezzolla, and D. H. Rischke, Bjorken flow in one-dimensional relativistic magnetohydrodynamics with magnetization, Phys. Rev. D **93**, 074022 (2016).
[20] S. Pu and D.-L. Yang, Transverse flow induced by inhomogeneous magnetic fields in the Bjorken expansion, Phys. Rev. D **93**, 054042 (2016).
[21] H. Li, X.-L. Sheng, and Q. Wang, Electromagnetic fields with electric and chiral magnetic conductivities in heavy ion collisions, Phys. Rev. C **94**, 044903 (2016).
[22] I. Siddique, X.-L. Sheng, and Q. Wang, Space-average electromagnetic fields and electromagnetic anomaly weighted by energy density in heavy-ion collisions, Phys. Rev. C **104**, 034907 (2021).
[23] U. Gursoy, D. Kharzeev, and K. Rajagopal, Magnetohydrodynamics, charged currents and directed flow in heavy ion collisions, Phys. Rev. C **89**, 054905 (2014).
[24] A. M. Poskanzer and S. A. Voloshin, Methods for analyzing anisotropic flow in relativistic nuclear collisions, Phys. Rev. C **58**, 1671 (1998).
[25] J.-Y. Ollitrault, Anisotropy as a signature of transverse collective flow, Phys. Rev. D **46**, 229 (1992).
[26] D. H. Rischke, Y. Pursun, J. A. Maruhn, H. Stoecker, and W. Greiner, The phase transition to the quark-gluon plasma and its effects on hydrodynamic flow, Acta Phys. Hung. A **1**, 309 (1995).
[27] H. Stoecker, Collective flow signals the quark gluon plasma, Nucl. Phys. A **750**, 121 (2005).
[28] U. Gürsoy, D. Kharzeev, E. Marcus, K. Rajagopal, and C. Shen, Charge-dependent flow induced by magnetic and electric fields in heavy ion collisions, Phys. Rev. C **98**, 055201 (2018).
[29] U. Gürsoy, D. E. Kharzeev, E. Marcus, K. Rajagopal, and C. Shen, Charge-dependent flow induced by electromagnetic fields in heavy ion collisions, Nucl. Phys. A **1005**, 121837 (2021).
[30] A. Dubla, U. Gürsoy, and R. Snellings, Charge-dependent flow as evidence of strong electromagnetic fields in heavy-ion collisions, Mod. Phys. Lett. A **35**, 2050324 (2020).
[31] G. Inghirami, M. Mace, Y. Hirono, L. Del Zanna, D. E. Kharzeev, and M. Bleicher, Magnetic fields in heavy ion collisions: Flow and charge transport, Eur. Phys. J. C **80**, 293 (2020).
[32] H. Song, Y. Zhou, and K. Gajdosova, Collective flow and hydrodynamics in large and small systems at the LHC, Nucl. Sci. Tech. **28**, 99 (2017).
[33] S. Chatterjee and P. Bozek, Interplay of drag by hot matter and electromagnetic force on the directed flow of heavy quarks, Phys. Lett. B **798**, 134955 (2019).
[34] L. Adamczyk *et al.* (STAR Collaboration), Beam-Energy Dependence of the Directed Flow of Protons, Antiprotons, and Pions in Au+Au Collisions, Phys. Rev. Lett. **112**, 162301 (2014).
[35] C. Alt *et al.* (NA49 Collaboration), Directed and elliptic flow of charged pions and protons in Pb + Pb collisions at 40*A* and 158*A* GeV, Phys. Rev. C **68**, 034903 (2003).
[36] Y. Pandit (STAR Collaboration), Directed flow of identified charged particles from the RHIC beam energy Sscan, Acta Phys. Pol. Suppl. **5**, 439 (2012).
[37] L. Adamczyk *et al.* (STAR Collaboration), Directed Flow of Identified Particles in Au + Au Collisions at $\sqrt{s_{NN}} = 200$ GeV at RHIC, Phys. Rev. Lett. **108**, 202301 (2012).
[38] Z.-Z. Han and J. Xu, Charge asymmetry dependence of the elliptic flow splitting in relativistic heavy-ion collisions, Phys. Rev. C **99**, 044915 (2019).
[39] L. Oliva, S. Plumari, and V. Greco, Directed flow of D mesons at RHIC and LHC: Non-perturbative dynamics, longitudinal bulk matter asymmetry and electromagnetic fields, J. High Energy Phys. 05 (2021) 034.
[40] A. I. Sheikh, D. Keane, and P. Tribedy, Testing the impact of electromagnetic fields on the directed flow of constituent quarks in heavy-ion collisions, Phys. Rev. C **105**, 014912 (2022).
[41] L. Yan and X.-G. Huang, Dynamical evolution of magnetic field in the pre-equilibrium quark-gluon plasma, arXiv:2104.00831.
[42] J.-J. Zhang, X. Zhang, G.-L. Peng, and Z.-P. Ren, A GPU-based general numerical framework for plasma simulations in terms of microscopic kinetic equations with full collision terms, Plasma Sci. Technol. **24**, 054007 (2022).
[43] J.-J. Zhang and H.-Z. Wu, ZMCintegral-v5: Support for integrations with the scanning of large parameter space on multi-GPUs, Comput. Phys. Commun. **251**, 107240 (2020).
[44] H.-Z. Wu, J.-J. Zhang, L.-G. Pang, and Q. Wang, ZMCintegral: A package for multi-dimensional Monte Carlo integration on multi-GPUs, Comput. Phys. Commun. **248**, 106962 (2020).
[45] J.-J. Zhang, H.-Z. Wu, S. Pu, G.-Y. Qin, and Q. Wang, Towards a full solution of relativistic Boltzmann equation for quark-gluon matter on GPUs, Phys. Rev. D **102**, 074011 (2020).
[46] J.-J. Zhang, J.-N. Chen, G.-L. Peng, T.-J. Du, and H.-Y. Xie, Jefigpu: Jefimenko's equations on gpu, Comput. Phys. Commun. **276**, 108328 (2022).
[47] H. De Vries, C. De Jager, and C. De Vries, Nuclear charge-density-distribution parameters from elastic electron scattering, At. Data Nucl. Data Tables **36**, 495 (1987).
[48] Q. Y. Shou, Y. G. Ma, P. Sorensen, A. H. Tang, F. Videbæk, and H. Wang, Parameterization of deformed nuclei for Glauber modeling in relativistic heavy ion collisions, Phys. Lett. B **749**, 215 (2015).
[49] P. Romatschke and M. Strickland, Collective modes of an anisotropic quark gluon plasma, Phys. Rev. D **68**, 036004 (2003).
[50] P. Romatschke and M. Strickland, Collective modes of an anisotropic quark-gluon plasma: II, Phys. Rev. D **70**, 116006 (2004).
[51] L. D. McLerran and R. Venugopalan, Computing quark and gluon distribution functions for very large nuclei, Phys. Rev. D **49**, 2233 (1994).
[52] L. D. McLerran and R. Venugopalan, Gluon distribution functions for very large nuclei at small transverse momentum, Phys. Rev. D **49**, 3352 (1994).
[53] E. Iancu, A. Leonidov, and L. D. McLerran, Nonlinear gluon evolution in the color glass condensate, Nucl. Phys. A **692**, 583 (2001).
[54] L. Keegan, A. Kurkela, A. Mazeliauskas, and D. Teaney, Initial conditions for hydrodynamics from weakly coupled pre-equilibrium evolution, J. High Energy Phys. 08 (2016) 171.

[55] A. Kurkela, A. Mazeliauskas, J.-F. Paquet, S. Schlichting, and D. Teaney, Effective kinetic description of event-by-event pre-equilibrium dynamics in high-energy heavy-ion collisions, Phys. Rev. C **99**, 034910 (2019).

[56] A. Kurkela, A. Mazeliauskas, J.-F. Paquet, S. Schlichting, and D. Teaney, Matching the Nonequilibrium Initial Stage of Heavy Ion Collisions to Hydrodynamics with QCD Kinetic Theory, Phys. Rev. Lett. **122**, 122302 (2019).

[57] A. Kurkela and A. Mazeliauskas, Chemical Equilibration in Hadronic Collisions, Phys. Rev. Lett. **122**, 142301 (2019).

[58] J. Churchill, L. Yan, S. Jeon, and C. Gale, Emission of electromagnetic radiation from the early stages of relativistic heavy-ion collisions, Phys. Rev. C **103**, 024904 (2021).

[59] L. Gribov, E. Levin, and M. Ryskin, Semihard processes in QCD, Phys. Rep. **100**, 1 (1983).

[60] S. S. Adler (PHENIX Collaboration) *et al.*, Identified charged particle spectra and yields in Au+Au collisions at $\sqrt{s_N N} = 200$ GeV, Phys. Rev. C **69**, 034909 (2004).

[61] J. Adams *et al.* (STAR Collaboration), Identified Particle Distributions in pp and Au+Au Collisions at $\sqrt{s_N N} = 200$ GeV, Phys. Rev. Lett. **92**, 112301 (2004).

[62] B. I. Abelev *et al.* (STAR Collaboration), Systematic measurements of identified particle spectra in pp, d^+ Au and Au+Au collisions from STAR, Phys. Rev. C **79**, 034909 (2009).

[63] S. A. Voloshin, A. M. Poskanzer, and R. Snellings, Collective phenomena in non-central nuclear collisions, Landolt-Bornstein **23**, 293 (2010).

[64] J. Brachmann, S. Soff, A. Dumitru, H. Stöcker, J. A. Maruhn, W. Greiner, L. V. Bravina, and D. H. Rischke, Antiflow of nucleons at the softest point of the equation of state, Phys. Rev. C **61**, 024909 (2000).

[65] R. J. M. Snellings, H. Sorge, S. A. Voloshin, F. Q. Wang, and N. Xu, Novel Rapidity Dependence of Directed Flow in High-Energy Heavy Ion Collisions, Phys. Rev. Lett. **84**, 2803 (2000).

[66] M. Bleicher and H. Stoecker, Anisotropic flow in ultra-relativistic heavy ion collisions, Phys. Lett. B **526**, 309 (2002).

[67] H. Petersen, Q. Li, X. Zhu, and M. Bleicher, Directed and elliptic flow in heavy ion collisions at GSI-FAIR and CERN-SPS, Phys. Rev. C **74**, 064908 (2006).

[68] Z. Wang, J. Zhao, C. Greiner, Z. Xu, and P. Zhuang, Incomplete electromagnetic response of hot QCD matter, Phys. Rev. C **105**, L041901 (2022).

[69] R. J. Fries, B. Muller, C. Nonaka, and S. A. Bass, Hadron production in heavy ion collisions: Fragmentation and recombination from a dense parton phase, Phys. Rev. C **68**, 044902 (2003).

[70] R. J. Fries, V. Greco, and P. Sorensen, Coalescence models for hadron formation from quark gluon plasma, Annu. Rev. Nucl. Part. Sci. **58**, 177 (2008).

[71] J. C. Dunlop, M. A. Lisa, and P. Sorensen, Constituent quark scaling violation due to Baryon number transport, Phys. Rev. C **84**, 044914 (2011).